Journal of Power Sources 194 (2009) 263–268

Contents lists available at ScienceDirect

Journal of Power Sources

journal homepage: www.elsevier.com/locate/jpowsour

Cathode reaction models and performance analysis of $Sm_{0.5}Sr_{0.5}CoO_{3-\delta}$–$BaCe_{0.8}Sm_{0.2}O_{3-\delta}$ composite cathode for solid oxide fuel cells with proton conducting electrolyte

Fei He, Tianzhi Wu, Ranran Peng*, Changrong Xia

CAS Key Laboratory of Materials for Energy Conversion, Department of Materials Science and Engineering, University of Science and Technology of China, Hefei 230026, Anhui, China

ARTICLE INFO

Article history:
Received 23 March 2009
Received in revised form 23 April 2009
Accepted 23 April 2009
Available online 3 May 2009

Keywords:
Solid oxide fuel cells
Cathode reaction models
Reaction order
Proton conductor
Polarization resistance

ABSTRACT

Cathode reaction models for solid oxide fuel cells with proton conducting electrolyte (H-SOFC) are proposed, and the reacting orders for each elementary step with respect to oxygen and water vapor partial pressure are calculated. The limiting steps of cathode reactions are investigated with $Sm_{0.5}Sr_{0.5}CoO_{3-\delta}$ (SSC)–$BaCe_{0.8}Sm_{0.2}O_{3-\delta}$ (BCS) composite cathodes. The results suggest that the migration of protons to TPBs and the surface diffusion of O^-_{ad} might be the limiting reactions for SSC–BCS composite cathodes in wet atmosphere, while the oxygen ions transferring into electrolyte, the reducing of O_{ad} to O^-_{ad}, and surface diffusion of O^-_{ad} might be the limiting reactions for SSC–BCS composite cathode in dry atmosphere.

1. Introduction

Solid oxide fuel cells with proton conducting electrolytes (H-SOFC) have attracted much attention for their great fuel utilization efficiency and simple fuel-recycling instruments [1–3]. In H-SOFC, hydrogen is oxidized at the anode to proton, which migrates selectively through the electrolyte to the cathode, and undergoes a half-cell reaction with oxygen to produce water. The overall half reactions at the anode and cathode could be expressed as Eqs. (1) and (2), respectively:

$$H_2 + 2O_O^\times \rightarrow 2OH_O^\bullet + 2e' \quad (1)$$

$$4OH_O^\bullet + O_2 + 4e' \rightarrow 2H_2O + 4O_O^\times \quad (2)$$

with water generated at cathode, the cathode reactions of H-SOFC differ a lot with those of cells with oxygen ion conducting electrolyte (O-SOFC), of which oxygen is reduced by the cathode to oxygen ions via the overall half-cell reaction:

$$O_2 + 4e' + 2V_O^{\bullet\bullet} \rightarrow 2O_O^\times \quad (3)$$

The difference in cathode reactions between H-SOFC and O-SOFC results in different cathode processes. But until now, few works have been reported on the cathodic processes, especially the limiting steps.

Uchida et al. [4] investigated the oxygen partial pressures (P_{O_2}) dependence of cathode polarization resistance (R_P) of Pt cathode, and proposed the elementary reaction steps for H-SOFC cathode. Yamaura et al. [5] investigated the polarization resistances of $La_{1-x}Sr_xFeO_{3-\delta}$ and Pt also by means of a current interruption method, and found that the rate-determining step of $La_{0.7}Sr_{0.3}FeO_{3-\delta}$ cathode was different from that of sputtered platinum cathode. And they indicated that further study was necessary to specify the limiting steps.

In this work, oxygen reactions at $Sm_{0.5}Sr_{0.5}CoO_{3-\delta}$ (SSC)–$BaCe_{0.8}Sm_{0.2}O_{3-\delta}$ (BCS) composite cathodes were investigated for H-SOFC with BCS electrolyte. The polarization resistance of SSC–BCS electrode was investigated by A.C. impedance as function of oxygen (P_{O_2}) and water vapor partial pressure (P_{H_2O}), respectively, to determine the rate-limiting steps. The cathode reaction mechanism for H-SOFC was proposed, and the dependence of reacting speed, accordingly the polarization resistance, on P_{O_2} and P_{H_2O} were calculated for each elementary step.

2. Experimental

Symmetric cells with $Sm_{0.5}Sr_{0.5}CoO_{3-\delta}$ (SSC)–$BaCe_{0.8}Sm_{0.2}O_{3-\delta}$ (BCS) composite cathodes were fabricated using screen-printing technique with $BaCe_{0.8}Sm_{0.2}O_{3-\delta}$ as the electrolyte. The proce-

* Corresponding author. Tel.: +86 551 3600594; fax: +86 551 3607475.
E-mail address: pengrr@ustc.edu.cn (R. Peng).

0378-7753/$ – see front matter © 2009 Elsevier B.V. All rights reserved.
doi:10.1016/j.jpowsour.2009.04.053

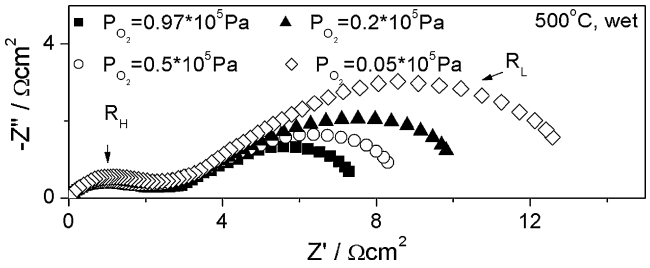

Fig. 1. Impedance spectra of an SSC–BCS electrode measured at 500 °C in humidified N_2–O_2 atmospheres with various oxygen partial pressures.

dures were summarized as follows: polycrystalline powders of SSC and BCS were prepared by a glycine-nitrate process as described in details previously [3,6]. BCS powders were pressed at 220 MPa into disks about 13 mm in diameter and 0.54 mm in thickness, and then sintered at 1500 °C for 5 h as electrolyte substrates. SSC and BCS powders were mixed at a weight ratio of 6:4 to prepare the print-ink with ethocel and abietyl alcohol as organic binder. The composite electrodes about 40 μm in thickness were formed by screen-printing the ink onto each side of the electrolyte substrate. The samples were fired at 1000 °C for 5 h in air to form the symmetric cells. Pt paste was applied onto the electrode surface as the current collector.

Symmetric cells were tested from 400 to 700 °C with a home-developed-cell-testing system by A.C. impedance method using an electrochemical workstation (IM6e, Zahner) under wet (~3% H_2O) or dry O_2–N_2 atmospheres. Measurements were conducted with the oxygen partial pressure ranging from 0.05 to 1.00 atm by mass-flow-meter (D08-2D/ZM) with the general atmosphere pressure (dry or wet) controlled at 1.00 atm. The water vapor partial pressure of 0.03, 0.06, 0.10, 0.15 and 0.20 atm was achieved by heating the bubble at different temperature. The frequency range for impedance measurements was from 0.01 Hz to 1 MHz. Curve fitting was performed using the Zview software.

3. Results

3.1. Properties of SSC–BCS composite electrodes under wet atmosphere

Fig. 1 presents the impedance spectra of SSC–BCS electrode measured at 500 °C in wet (~3% H_2O) O_2–N_2 atmosphere with oxygen partial pressure ranging from 0.05×10^5 to 0.97×10^5 Pa. Two depressed arcs are observed in each spectrum, a small high-frequency arc and a large low-frequency arc with relaxation frequencies of 24 kHz and 0.1 Hz at 500 °C, respectively, implying that there are two rate-limiting steps. An equivalent circuit composed of two RQ elements (R_HQ_H) (R_LQ_L) are proposed to resolve these spectra, where R represents the polarization resistance, Q represents the constant phase element, and the subscripts H and L correspond to the high- and low-frequency arc, respectively. At oxygen partial pressure (P_{O_2}) of 0.97×10^5 Pa, the fitted R_H and R_L is 2.07 and 5.23 Ω cm^2, respectively. With the decrease of oxygen partial pressure, R_L increase largely, while R_H keeps almost constant. And at P_{O_2} of 0.05×10^5 Pa, R_H and R_L are 2.17 and 10.78 Ω cm^2, respectively, suggesting that the resistance associated to the low-frequency arc is the main contribution to the polarization resistance at 500 °C. The values of capacitance at 500 °C are about 0.5 μF cm^{-1} and 0.4 F cm^{-1} for the high- and low-frequency arc, respectively.

The dependence of R_H and R_L on oxygen partial pressure (P_{O_2}) are presented in the usual form, $R_i \prec (P_{O_2})^{-m}$, where m is also deemed as reaction order of R_i with respect to P_{O_2}. As shown in Fig. 2, R_H is almost independent on oxygen partial pressure over the entire

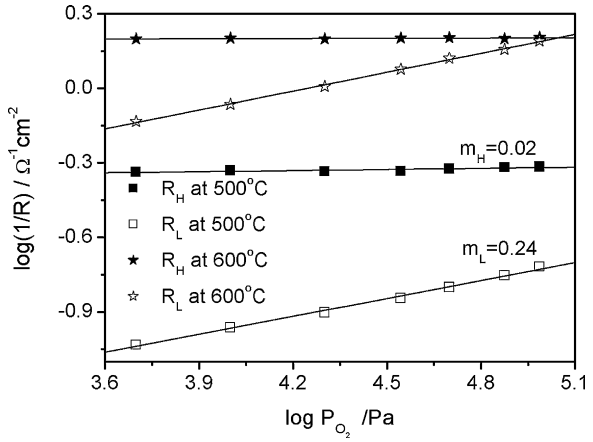

Fig. 2. Oxygen partial pressure (P_{O_2}) dependence of high-frequency resistance (R_H, solid) and low-frequency resistance (R_L, open) measured in humidified N_2–O_2 atmosphere at 500 and 600 °C, respectively.

P_{O_2} range measured with fitted m_H very close to zero, 0.02 ± 0.01 on average, suggesting that neither atomic oxygen nor molecular oxygen is involved in this step. While for R_L, a linear increase of $\log(1/R_L)$ is observed with the increase of oxygen partial pressure, and the fitted m_L is close to 1/4 (0.24 ± 0.01).

Arrhenius plots of R_H and R_L at different oxygen partial pressures were shown in Fig. 3 to determine the activation energy for reacting species. Within the tested temperature, R_H was independent on oxygen partial pressures, and the simulated activation energy was 0.60 eV, quite close to that of proton conducting in doped $BaCeO_3$ [7–10], about 0.4–0.65 eV, implying that the reaction corresponding to the high-frequency arc might be proton involved. Although R_L values increased with the decrease of oxygen partial pressures, its activation energies are about 1.18 eV and also independent of the oxygen partial pressures. The high activation energy of R_L suggests that R_L decreases more rapidly with the testing temperature than R_H. At temperature below 600 °C with oxygen partial pressure of 0.97×10^5 Pa, R_L exceeds R_H and becomes the dominating contribution of electrode resistance.

The dependence of R_H and R_L on the water vapor partial pressure, P_{H_2O}, are also investigated with P_{O_2} controlled at 0.20×10^5 Pa, and no additional arcs besides the high- and the low-frequency arc are observed within the measured water vapor pressure range, as shown in Fig. 4. The dependence of R_H and R_L on P_{H_2O} are quite different with those on P_{O_2}. At 500 °C with P_{H_2O} increased from

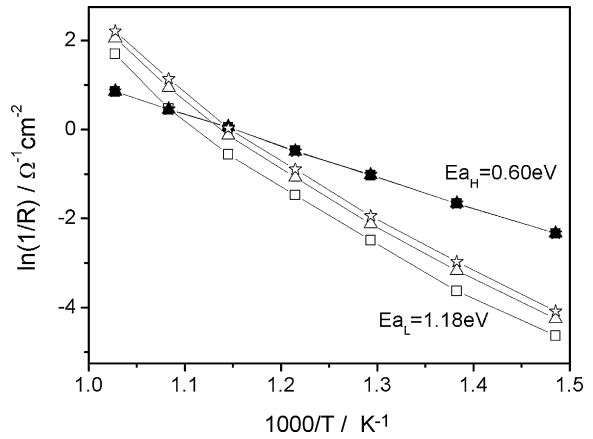

Fig. 3. Arrhenius plots of R_H (solid) and R_L (open) measured in humidified N_2–O_2 atmosphere with oxygen partial pressure $P_{O_2} = 0.20$ atm (■, □), 0.5 atm (▲, △), and 0.97 atm (★, ☆), respectively.

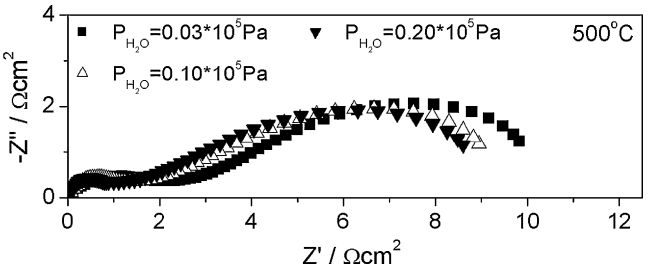

Fig. 4. Impedance spectra of SSC–BCS electrode measured at 500 °C in 20% O_2–N_2 atmosphere with various vapor partial pressures.

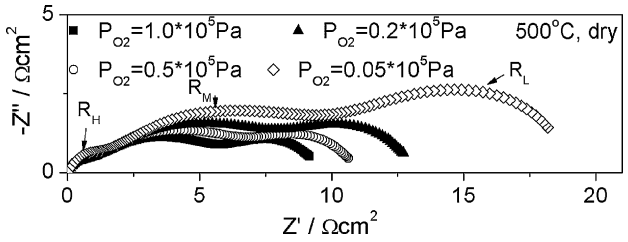

Fig. 6. Impedance spectra of SSC–BCS electrode measured at 500 °C in dry N_2–O_2 atmosphere with various oxygen partial pressures.

0.03×10^5 Pa to 0.20×10^5 Pa, R_H reduces from 2.16 to 0.90 Ω cm^2, while R_L keeps almost constant at 7.89 Ω cm^2, suggesting that H_2O is involved in the steps corresponding to the high-frequency arc but not in that to the low-frequency arc.

The reaction orders with respect to P_{H_2O}, n, for the electrode reactions are determined from the slope of R_H and R_L curves, respectively, as shown in Fig. 5. The reaction order for the high-frequency reaction, n_H, is close to 1/2 (0.46 ± 0.01), while the reaction order for the low-frequency reaction, n_L, appears close to zero (0.01 ± 0.01). And both n_H and n_L is independent of temperature.

Thus the dependence of high-frequency resistance and low-frequency resistance on P_{O_2} and P_{H_2O} can be concluded as Eqs. (4) and (5), and their detailed steps will be specified by later discussion:

$$R_H \prec P_{O_2}^0 P_{H_2O}^{-1/2} \quad (4)$$

$$R_L \prec P_{O_2}^{-1/4} P_{H_2O}^0 \quad (5)$$

3.2. Properties of SSC–BCS composite electrodes under dry atmosphere

The properties of SSC–BCS composite electrodes are also investigated under dry O_2–N_2 atmosphere, in which $BaCe_{0.8}Sm_{0.2}O_{3-\delta}$ (BCS) is a pure oxygen ion conductor. The change of conducting species from proton to oxygen ions resulted in quite different cathode reactions. Fig. 6 presents the impedance spectra for the SSC–BCS electrode measured at 500 °C in dry O_2–N_2 atmosphere with various oxygen partial pressures. Unlike the impedance spectra tested under wet atmosphere, there are three depressed arcs in each spectrum, noted as high-frequency arc, middle-frequency arc and low-frequency arc, respectively. With the decrease of P_{O_2}, the length of middle- and low-frequency arcs increase obviously, while that of high-frequency arc is the same. Detail analysis of these spectra was conducted using the equivalent circuit with three RQ elements (R'_H Q_H)(R'_M Q_M)(R'_L Q_L), where R' presents the polarization resistance, and the subscripts H, M and L denote the process corresponding to high-, middle- and low-frequency arc, respectively. The fitted capacity for high-, middle- and low-frequency arc are 1.43×10^{-7}, 1×10^{-4} and 0.704F with the relaxation frequency 130 K, 180 and 0.18 Hz, respectively. Tested at 500 °C, R'_H, R'_M and R'_L were 1.14, 6.98, and 5.26 Ω cm^2, respectively, with P_{O_2} of 0.20×10^5 Pa.

Fig. 7 presents the dependence of R'_H, R'_M and R'_L on the oxygen partial pressure tested at 500 °C in dry N_2–O_2 atmosphere. As shown, the reaction order with respect to oxygen partial pressure, is close to 0 (0.0 ± 0.01), 3/8 (0.34 ± 0.02) and 1/4 (0.19 ± 0.02) for R'_H, R'_M and R'_L, respectively. The activation energies were also independent on oxygen partial pressure, about 1.28, 1.00 and 1.17 eV for R'_H, R'_M and R'_L, respectively. The activation energies for R'_H is almost twice of that in wet atmosphere, suggesting the different reacting species in wet and dry atmosphere. It should be noted that the reaction order and the activation energy are almost the same in both wet and dry atmospheres for low-frequency resistances, suggesting similar reacting mechanism. The dependence of R'_H, R'_M and R'_L on P_{O_2} can be summarized as Eqs. (6)–(8):

$$R'_H \prec P_{O_2}^0 \quad (6)$$

$$R'_M \prec P_{O_2}^{-3/8} \quad (7)$$

$$R'_L \prec P_{O_2}^{-1/4} \quad (8)$$

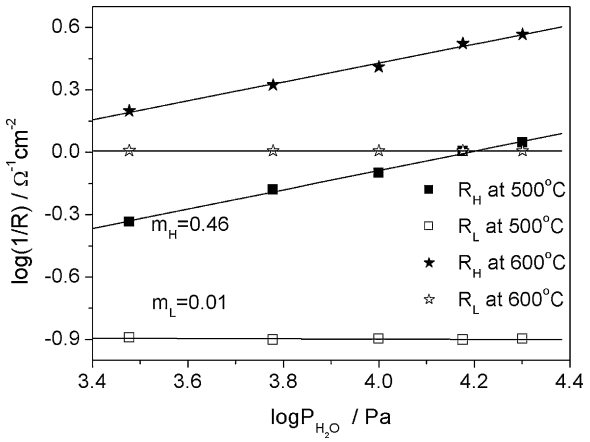

Fig. 5. Vapor partial pressure (P_{H_2O}) dependence of high-frequency resistance (R_H, solid) and low-frequency resistance (R_L, open) in humid 20% O_2–N_2 atmosphere at 500 and 600 °C, respectively.

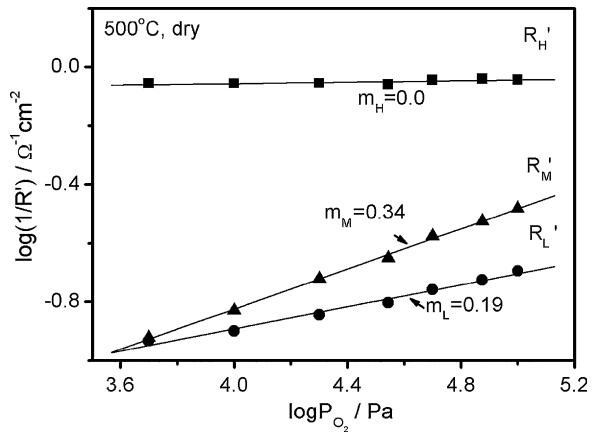

Fig. 7. Oxygen partial pressure (P_{O_2}) dependence of high-frequency resistance (R'_H), middle-frequency resistance (R'_M), and low-frequency resistance (R'_L) in dry N_2–O_2 atmosphere measured at 500 °C.

4. Discussion

4.1. Cathode reaction models and data analysis in wet atmospheres

The cathode reactions of H-SOFCs are more complex than those of O-SOFCs due to the formation of H_2O at the cathodes. And the cathode reactions of H-SOFCs might consist of several steps including: (1) surface dissociative adsorption and diffusion of oxygen along with charge transfer; (2) proton migration to triple phase boundaries (TPBs); and (3) the formation and desorption of H_2O. In Uchita's [4] reaction models, the proposed cathode steps mainly came from those of O-SOFC, and the individual steps of proton reacting were seldom considered. In this work, detailed reacting steps for the cathode of H-SOFCs are proposed, and the reacting rate for each step are calculated as function of oxygen water vapor partial pressures. The elementary steps are expressed as Steps 1–8:

Step 1

$$O_{2(g)} \rightarrow 2O_{ad}$$

Step 2

$$O_{ad} + e^- \rightarrow O^-_{ad}$$

Step 3

$$O^-_{ad} \rightarrow O^-_{TPB}$$

Step 4

$$O^-_{TPB} + e^- \rightarrow O^{2-}_{TPB}$$

Step 5

$$OH^{\bullet}{}_{O\,electrolyte} \rightarrow H^+_{TPB} + O^{\times}_{O}$$

Step 6

$$H^+_{TPB} + O^{2-}_{TPB} \rightarrow OH^-_{TPB}$$

Step 7

$$H^+_{TPB} + OH^-_{TPB} \rightarrow H_2O_{TPB}$$

Step 8

$$H_2O_{TPB} \rightarrow H_2O(g)$$

where Steps 1–2 describe the dissociative adsorption of oxygen to O^-; Step 3 describes the diffusion of O^- species along the SSC surface to the triple surface boundaries (TPBs); Step 5 describes the transfer of protons from the electrolyte ($OH^{\bullet}{}_{O\,electrolyte}$) to the TPBs; Steps 6 and 7 describe the reaction of protons and oxygen species; and Step 8 is desorption of H_2O from TPBs into gas phase. In this model, the oxygen dissociated adsorption and diffusion, Steps 1–4, are similar to that in O-SOFCs [11]. The rate equations corresponding to Steps 1–8 can be calculated by $r = r_{forward} - r_{reverse}$, and the details are shown as follows:

$$r_1 = k_i P_{O_2} - k'_1 a^2_{O_{ad}} \tag{9}$$

$$r_2 = k_2 a_{O_{ad}} \exp\left(-\frac{FE}{2RT}\right) - k'_2 a_{O^-_{ad}} \exp\left(\frac{FE}{2RT}\right) \tag{10}$$

$$r_3 = k_3 a_{O^-_{ad}} - k'_3 a_{O^-_{TPB}} \tag{11}$$

$$r_4 = k_4 a_{O^-_{TPB}} \exp\left(-\frac{FE}{2RT}\right) - k'_4 a_{O^{2-}_{TPB}} \exp\left(\frac{FE}{2RT}\right) \tag{12}$$

$$r_5 = k_5 a_{OH_{O\,electrolyte}{}^{\bullet}} - k'_5 a_{H^+_{TPB}} \tag{13}$$

$$r_6 = k_6 a_{H^+_{TPB}} a_{O^{2-}_{TPB}} - k'_6 a_{OH^-_{TPB}} \tag{14}$$

$$r_7 = k_7 a_{H^+} a_{OH^-_{TPB}} - k'_7 a_{H_2O_{TPB}} \tag{15}$$

$$r_8 = k_8 a_{H_2O_{TPB}} - k'_8 P_{H_2O} \tag{16}$$

where r_i is the general reaction rate with the subscripts denoting the step number; k_i and k'_i are the rate constants for the forward and backward reactions, respectively; a_M represent the activity of appointed species marked as the subscript; and R, T and F is the gas constant, absolute temperature and the Faraday constant, respectively. The symmetry coefficient, β, is assumed to be 1/2. E is the electrode potential generated by Nernst equation, as shown in Eq. (17). It should be noted that the protons in the electrolyte is generated by the incorporation of water into the BCS electrolyte, as shown in Eq. (18), and thus $a_{OH^{\bullet}{}_{O\,electrolyte}}$ can be calculated by Eq. (19):

$$E_{eq} = const + \left(\frac{RT}{4F}\right) \ln P_{O_2} \tag{17}$$

$$H_2O(g) + O^{\times}_{O} + V_O^{\bullet\bullet} \Leftrightarrow 2OH_O^{\bullet} \tag{18}$$

$$a_{OH^{\bullet}{}_{O\,electrolyte}} = \left(\frac{1}{k_H}\right)^{1/2} P^{1/2}_{H_2O} \tag{19}$$

where k_H is the rate constant for the balance reactions of Eq. (18).

Thus the reacting rate of Steps 1–8 can be given as function of P_{O_2} and P_{H_2O}. For example, if Step 7 was assumed to be the rate-determining step and Steps 1–6 and 8 were in virtual equilibrium, the rate of Step 7 could be calculated by figuring out a_{H^+}, $a_{OH^-_{TPB}}$ and $a_{H_2O_{TPB}}$:

(1) a_{H^+}: Submitting Eq. (19) into Eq. (13), we obtained the activity of protons at TPBs:

$$a_{H^+_{TPB}} = \left(\frac{1}{k_H}\right)^{1/2} \left(\frac{k_5}{k'_5}\right) P^{1/2}_{H_2O} \tag{20}$$

(2) $a_{H_2O_{TPB}}$: From Eq. (16), the activity of adsorbed H_2O at TPBs can be expressed as function of P_{H_2O}, as shown in Eq. (21):

$$a_{H_2O_{TPB}} = \left(\frac{k'_8}{k_8}\right) P_{H_2O} \tag{21}$$

(3) $a_{OH^-_{TPB}}$: The activity of OH^- at TPBs can be calculated from the equilibrium of Eq.(9), (10), (11), (12) and (14). From Eq. (9), the activity of dissociated oxygen (O_{ad}) can be obtained as Eq. (22):

$$a_{O_{ad}} = \left(\frac{k_1}{k'_1}\right)^{1/2} P^{1/2}_{O_2} \tag{22}$$

Combining Eqs. (22) and (10), we obtain:

$$a_{O^-_{ad}} = \left(\frac{k_2}{k'_2}\right)\left(\frac{k_1}{k'_1}\right)^{1/2} P^{1/2}_{O_2} \exp\left(-\frac{FE}{RT}\right) \tag{23}$$

Substituting Eq. (23) into Eq. (11) gives:

$$a_{O^-_{TPB}} = \left(\frac{k_1}{k'_1}\right)^{1/2} \left(\frac{k_2}{k'_2}\right)\left(\frac{k_3}{k'_3}\right) P^{1/2}_{O_2} \exp\left(-\frac{FE}{RT}\right) \tag{24}$$

Substituting Eq. (24) into Eq. (12) gives:

$$a_{O^{2-}_{TPB}} = \left(\frac{k_4}{k'_4}\right)\left(\frac{k_3}{k'_3}\right)\left(\frac{k_2}{k'_2}\right)\left(\frac{k_1}{k'_1}\right)^{1/2} P_{O_2}^{1/2} \exp\left(-\frac{2FE}{RT}\right) \quad (25)$$

Substituting Eqs. (20) and (25) into Eq. (14) gives:

$$a_{OH^-_{TPB}} = \left(\frac{1}{k_H}\right)^{1/2}\left(\frac{k_5}{k'_5}\right)\left(\frac{k_6}{k'_6}\right) P_{H_2O}^{1/2} \cdot \left(\frac{k_4}{k'_4}\right)\left(\frac{k_3}{k'_3}\right)\left(\frac{k_2}{k'_2}\right)\left(\frac{k_1}{k'_1}\right)^{1/2} P_{O_2}^{1/2} \exp\left(-\frac{2FE}{RT}\right) \quad (26)$$

Thus, the steady state reaction rate of Step 7 can be calculated by substituting Eqs. (20), (21) and Eq. (26) into Eq. (15), as shown in Eq. (27):

$$r_7 = k'_7 P_{H_2O} - k_7\left(\frac{1}{k}\right)\left(\frac{k_5}{k'_5}\right)^2 P_{H_2O} \cdot \left(\frac{k_4}{k'_4}\right)\left(\frac{k_3}{k'_3}\right)\left(\frac{k_2}{k'_2}\right)\left(\frac{k_1}{k'_1}\right)^{1/2} P_{O_2}^{1/2} \exp\left(-\frac{2FE}{RT}\right) \quad (27)$$

Thus the forward and the reverse reaction rate for Step 7 can be expressed as Eqs. (28) and (29), respectively.

$$r_{forward} = k'_7 P_{H_2O} \quad (28)$$

$$r_{reverse} = k_7\left(\frac{1}{k}\right)\left(\frac{k_5}{k'_5}\right)^2 P_{H_2O} \cdot \left(\frac{k_4}{k'_4}\right)\left(\frac{k_3}{k'_3}\right)\left(\frac{k_2}{k'_2}\right)\left(\frac{k_1}{k'_1}\right)^{1/2} P_{O_2}^{1/2} \exp\left(-\frac{2FE}{RT}\right) \quad (29)$$

As shown in Eq. (28), the forward reaction rate is the function of P_{H_2O} and independent of P_{O_2}. Substituting the Nernst equation, Eq. (17) into Eq. (29), the reverse reaction rate is obtained as Eq. (30), which is also the function of P_{H_2O} and independent of P_{O_2}.

$$r_{reverse} = k_7\left(\frac{1}{k}\right)\left(\frac{k_5}{k'_5}\right)^2 P_{H_2O} \cdot \left(\frac{k_4}{k'_4}\right)\left(\frac{k_3}{k'_3}\right)\left(\frac{k_2}{k'_2}\right)\left(\frac{k_1}{k'_1}\right)^{1/2} \exp\left(-\frac{2Fconst}{RT}\right) \quad (30)$$

Thus the reaction order for Step 7 with respect to oxygen partial pressure and water vapor partial pressure are 0 and 1, respectively.

We now consider Step 3 as the rate-determining step and assuming that Steps 1, 2, 4–8 were in virtual equilibrium. The reaction rate of Step 3 can be calculated by figuring out $a_{O^-_{ad}}$ and $a_{O^-_{TPB}}$.

(1) $a_{O^-_{ad}}$: Calculated from the equilibrium of Eqs. (9) and (10), as shown in Eq. (23):

(2) $a_{O^-_{TPB}}$: Substituting Eqs. (20), (21) into Eq. (15) gives:

$$a_{OH^-_{TPB}} = k^{1/2}\left(\frac{k'_5}{k_5}\right)\left(\frac{k'_7}{k_7}\right)\left(\frac{k'_8}{k_8}\right) P_{H_2O}^{1/2} \quad (31)$$

Submitting Eqs. (20) and (31), into Eq. (14), we obtained:

$$a_{O^{2-}_{TPB}} = k\left(\frac{k'_5}{k_5}\right)^2\left(\frac{k'_6}{k_6}\right)\left(\frac{k'_7}{k_7}\right)\left(\frac{k'_8}{k_8}\right) \quad (32)$$

Table 1
Elementary cathode reaction steps and their reaction order with respect to oxygen partial pressure (m) and water vapor partial pressure (n), for solid oxide fuel cells with proton conducting electrolyte.

	Elementary reaction	m	n
Step 1	$O_{2(g)} \rightarrow 2O_{ad}$	1	0
Step 2	$O_{ad} + e^- \rightarrow O^-_{ad}$	3/8	0
Step 3	$O^-_{ad} \rightarrow O^-_{TPB}$	1/4	0
Step 4	$O^-_{TPB} + e^- \rightarrow O^{2-}_{TPB}$	0	0
Step 5	$H^+_{electrolyte} \rightarrow H^+_{TPB}$	0	1/2
Step 6	$H^+_{TPB} + O^{2-}_{TPB} \rightarrow OH^-_{TPB}$	0	1/2
Step 7	$H^+_{TPB} + OH^-_{TPB} \rightarrow H_2O_{TPB}$	0	1
Step 8	$H_2O_{TPB} \rightarrow H_2O(g)$	0	1

Combining Eqs. (32) and (12), we obtained:

$$a_{O^-_{TPB}} = k\left(\frac{k'_4}{k_4}\right)\left(\frac{k'_5}{k_5}\right)^2\left(\frac{k'_6}{k_6}\right)\left(\frac{k'_7}{k_7}\right)\left(\frac{k'_8}{k_8}\right)\exp\left(\frac{FE}{RT}\right) \quad (33)$$

We obtained the reaction rate of Step 7 by substituting Eqs. (33) and (23) into Eq. (11):

$$r_3 = nFk'_3 k\left(\frac{k'_4}{k_4}\right)\left(\frac{k'_5}{k_5}\right)^2\left(\frac{k'_6}{k_6}\right)\left(\frac{k'_7}{k_7}\right)\left(\frac{k'_8}{k_8}\right)\exp\left(\frac{FE}{RT}\right) - nFk_3\left(\frac{k_2}{k'_2}\right)\left(\frac{k_1}{k'_1}\right)^{1/2} P_{O_2}^{1/2}\exp\left(-\frac{FE}{RT}\right) \quad (34)$$

Substituting the Nernst equation into Eq. (34), we obtained:

$$r_3 = nFk'_3 k\left(\frac{k'_4}{k_4}\right)\left(\frac{k'_5}{k_5}\right)^2\left(\frac{k'_6}{k_6}\right)\left(\frac{k'_7}{k_7}\right)\left(\frac{k'_8}{k_8}\right)\exp\left(\frac{Fconst}{RT}\right) P_{O_2}^{1/4} - nFk_3\left(\frac{k_2}{k'_2}\right)\left(\frac{k_1}{k'_1}\right)^{1/2}\exp\left(-\frac{Fconst}{RT}\right) P_{O_2}^{1/4} \quad (35)$$

Thus, the dependence of r_3 on P_{O_2} and P_{H_2O} is derived as Eq. (36). And the reaction rate is determined as 1/4 and 0 with respect to P_{O_2} and P_{H_2O}, respectively.

$$r_3 \propto P_{O_2}^{1/4} P_{H_2O}^0 \quad (36)$$

And the reacting speed of other elementary step can be calculated in the same way, as shown in Table 1, where m and n refers to the reacting order for each step with respect to P_{O_2} and P_{H_2O}, respectively. As shown, the dependence of reacting speeds for Steps 1–4 on P_{O_2} is similar to those in O-SOFC proposed by Kim et al. [11], indicating similar reaction mechanism for oxygen dissociated adsorption and diffusion. It also should be noticed that Steps 5 and 6 have the same dependence on P_{O_2} and P_{H_2O}, implying that they cannot be discerned by only investigating their dependence on oxygen and water vapor partial pressure.

4.2. Data analysis for SSC–BCS in wet and dry atmosphere

In wet atmosphere, the low-frequency resistance is independent of P_{H_2O}, while proportionate to P_{O_2} with the reaction order of 1/4, as shown in Eq. (4). As referred to Table 1, Step 3 has the same dependence on P_{O_2} with the low-frequency resistance, suggesting that the low-frequency arc might correspond to the surface diffusion of O^-_{ad}. The activation energy of low-frequency resistance is 1.17 eV, close to that in SSC-LSGM [12], which is deemed corresponding to the surface dissociative adsorption and diffusion of oxygen. This further confirms the surface diffusion of O^-_{ad} in low-frequency reaction. While the high-frequency resistance is proportionate to P_{H_2O} with the reaction order of 1/2, and is independent of P_{O_2}. As shown in

Table 1, both Steps 5 and 6 might be the corresponding steps, which describe the protons transfer from the bulk of electrolyte to TPBs and the reacting of protons at TPBs with O^{2-} to form OH^-, respectively. Thus the specific step corresponding to the high-frequency arc cannot be discerned simply from its dependence on oxygen and water vapor partial pressure. Yet, considering the activation energy of high-frequency resistance of 0.6 eV, Step 5 is more promising, since the generating energy of OH^- is usually about an order lower than that of proton migration [13]. Thus the migration of protons to TPBs and the surface diffusion of O^-_{ad} might be the limiting reactions for SSC–BCS composite cathode in wet atmosphere.

In dry atmosphere, the low-frequency resistances have almost the same the reaction order and the activation energy with that in wet atmospheres. This suggests surface diffusion of O^-_{ad} might also be the corresponding reactions for low-frequency arc in dry atmosphere, which accords with that for O-SOFC previously [12]. Although the high-frequency resistances have the same reaction orders with respect to P_{O_2}, their activation energy is 1.28 eV, about twice of that in wet atmosphere, suggesting different conducting species. For O-SOFC, the high-frequency resistance is usually related to the oxygen ion transfer from the TPB into the electrolyte lattice, as described in Eq. (37), because of its independence on oxygen partial pressure[11,12]. This differs a lot from that in H-SOFC, suggesting that oxygen ions transition might the corresponding steps for SSC–BCS in dry atmosphere:

$$O^{2-}_{TPB} + V_O \cdot\cdot \rightarrow O^{\times}_{O} \quad (37)$$

While the reactions order for middle-frequency resistance with respect to P_{O_2} is 3/8, which was not observed in the spectra in wet atmosphere. And reducing of O_{ad} to O^-_{ad}, as shown in Table 1, is proposed to the corresponding step for middle-frequency arc. Thus the limiting reactions for SSC–BCS composite cathode in dry atmosphere should be the oxygen ions transfer from TPBs into electrolyte, the reducing of O_{ad} to O^-_{ad}, and surface diffusion of O^-_{ad}.

5. Conclusion

Reaction models for solid oxide fuel cells with proton conducting electrolyte (H-SOFC) are proposed for composite cathodes in this work, and the rate of each elementary step is calculated as function of oxygen and water vapor partial pressure, as shown in Table 1.

Using $Sm_{0.5}Sr_{0.5}CoO_{3-\delta}$ (SSC)–$BaCe_{0.8}Sm_{0.2}O_{3-\delta}$ (BCS) composite cathode, the impedance spectra under various atmosphere were measured to investigate the cathode limiting reactions for H-SOFC. Two arcs were observed for SSC–BCS under wet conditions. The high-frequency resistances are proportionate to $(P_{H_2O})^{-1/2}$ and independent of P_{O_2} with the activation energy of 0.6 eV, suggesting that the migration of protons to TPBs might be the corresponding step. While the low-frequency resistances are proportionate to $(P_{O_2})^{-1/4}$ and independent of P_{H_2O}, which might correspond to the surface diffusion of O^-_{ad}.

While in dry atmosphere, where BCS is a pure oxygen ion conductor, there were three arcs in the impedance spectra. The high-frequency resistances are independent of P_{O_2} with the activation energy of 1.28 eV, which might correspond to the oxygen ions transferring into electrolyte. The middle-frequency resistances are proportionate to $(P_{O_2})^{-3/8}$, and thus, the reducing of O_{ad} to O^-_{ad} might be the corresponding step. While the low-frequency resistance is proportionate to $(P_{O_2})^{-1/4}$, similar to that in wet atmosphere, which might correspond to surface diffusion of O^-_{ad}.

Acknowledgements

This work was supported by the Natural Science Foundation of China (50602043, 50730002), and by the Anhui Natural Science Foundation (KJ2007A090).

References

[1] K.D. Kreuer, Annu. Rev. Mater. Res. 33 (2003) 333–359.
[2] D. Hirabayashi, A. Tomita, S. Teranishi, T. Hibino, M. Sano, Solid State Ionics 176 (2005) 881–887.
[3] R. Peng, Y. Wu, L. Yang, Z. Mao, Solid State Ionics 177 (2006) 389–393.
[4] H. Uchida, S. Tanaka, H. Iwahara, J. Appl. Electrochem. 15 (1995) 93–97.
[5] H. Yamaura, T. Ikuta, H. Yahiro, G. Koda, Solid State Ionics 176 (2005) 269–274.
[6] W. Zhu, C.R. Xia, J. Fan, R.R. Peng, G.Y. Meng, J. Power Sources 160 (2006) 897–902.
[7] M. Amsif, D. Marrero-López, A. Magrasó, J. Peña-Martínez, J.C. Ruiz-Morales, P. Núñez, J. Eur. Ceram. Soc. 29 (2009) 131–138.
[8] J.-X. Wang, L.-P. Li, B.J. Campbell, Z. Lv, Y. Ji, Y.-F. Xue, W.-H. Su, Mater. Chem. Phys. 86 (2004) 150–155.
[9] W. Munch, G. Seifert, K.D. Kreuer, J. Maier, Solid State Ionics 97 (1997) 39–44.
[10] M. Oishi, S. Akoshima, K. Yashiro, K. Sato, J. Mizusaki, T. Kawada, Solid State Ionics 179 (2008) 2240–2247.
[11] J. Kim, G. Kim, J. Moon, Y. Park, W. Lee, K. Kobayashi, M. Nagai, C. Kim, Solid State Ionics 143 (2001) 379–389.
[12] S.Z. Wang, X. Liu, Acta Physico-Chimica Sinica 20 (5) (2004) 472–477.
[13] J. Li, Z. Zhao, A. Kazakov, F.L. Dryer, Int. J. Chem. Kinet. 36 (2004) 566–575.